



Cite this: *J. Mater. Chem. A*, 2025, **13**, 29050

## Electrodeposition of reactive polymer networks for conformal ultrathin coatings amenable to post-deposition functionalization

Wenlu Wang, <sup>a</sup> Yuanzhi Li, <sup>b</sup> Anton B. Resing, <sup>a</sup> Jin Yan, <sup>a</sup> Zhaoyi Zheng <sup>a</sup> and Jörg G. Werner <sup>\*abc</sup>

Functional thin coatings are crucial in modern and emerging technologies, providing specified surface properties and protection, thereby influencing the performance and lifetime of materials and devices. The electrodeposition of polymer networks (EPoN) has recently been reported as a facile and potentially broadly applicable method to fabricate conformal polymeric ultrathin films on conductive substrates with arbitrary shapes and surface topography under mild solution conditions. In this work, a new generation of EPoN is introduced that utilizes a chemically reactive polymer appended by a small fraction of a electrochemical crosslinker as side groups. This EPoN iteration eliminates the need for precise end-group functionalization, enables the tuning of crosslink density and film thickness independent of polymer size, and the resulting reactive ultrathin films are amenable to post-deposition modification with desired functionalities using facile click-chemistry. To demonstrate this concept, we electrodeposit polyisoprene with small side-group fractions of the oxidative crosslinker phenol (<5%) as a thiol–ene-reactive polymer-network coating. The EPoN-derived ultrathin films are tunable and uniform with a thickness in the 100s of nanometers depending on phenol fraction and electrodeposition potential, and show a conformal morphology on complex porous electrode architectures. We further demonstrate post-EPoN functionalization of the ultrathin polyisoprene coatings with thiol–ene chemistry.

Received 12th May 2025  
Accepted 31st July 2025

DOI: 10.1039/d5ta03811a  
[rsc.li/materials-a](http://rsc.li/materials-a)

<sup>a</sup>Division of Materials Science and Engineering, Boston University, Boston MA, USA  
E-mail: [jgwerner@bu.edu](mailto:jgwerner@bu.edu)

<sup>b</sup>Department of Mechanical Engineering, Boston University, Boston MA, USA  
<sup>c</sup>Department of Chemistry, Boston University, Boston MA, USA



Jörg G. Werner

*Jörg G. Werner received his Diplom in Chemistry from the Johannes Gutenberg University in 2011 and his PhD in Chemistry and Chemical Biology from Cornell University in 2016. After postdoctoral research at Harvard University, he started his independent research group at Boston University as an Assistant Professor of Mechanical Engineering and Materials Science and Engineering in 2020. His research focuses on spatially controlled synthesis utilizing bottom-up polymer self-assembly and phase separation, as well as electrochemical methods to study composition–structure–performance relationships across scales of mesostructured architected materials and devices applied to energy and sustainability technologies.*

## Introduction

Ultrathin coatings are surface-covering films with thickness ranging from a few to hundreds of nanometers that play a pivotal role in defining the surface properties and functionality of materials. This includes regulating mass and energy transfer between two phases, controlling the wetting behavior of surfaces, or providing mechanical and chemical protection from the surrounding environment. For example, grafting a biocompatible molecule monolayer on tubing or medical devices alters the surface chemistry and reduces fouling of undesired protein and immune response.<sup>1</sup> Functional coatings on planar or non-planar substrates can endow the surface with distinct purposes such as attracting or repelling of water or oil,<sup>2</sup> as well as self-cleaning<sup>3</sup> or anti-corrosion<sup>4</sup> properties. Due to the tailorabile pore sizes and architectures as well as the extensive surface area, three-dimensional (3D) and porous material and device architectures are emerging as essential features in many advanced technologies including energy storage and conversion,<sup>5–7</sup> catalysis,<sup>8,9</sup> sensors,<sup>10</sup> and separation.<sup>11</sup> Coatings from polymer networks in particular offer high chemical versatility through the selection of their monomer functionality, both in terms of side groups and backbone, and allow for precise modulation of mechanical and transport properties *via* control over network topology and backbone architecture,

rendering them the dominant choice in classic externally applied coatings.<sup>12</sup> However, while the combination of 3D and porous substrates with functional ultrathin polymer-network coatings offers vast opportunities for advanced hierarchical functional materials in scientific and technological innovations, their precise fabrication remains challenging and limited in types of polymers that can be conformally and uniformly deposited.

For polymer thin films on non-planar substrates, initiated and oxidative chemical vapor deposition (i/o-CVD) have proven themselves suitable for low aspect ratio topographies.<sup>13–15</sup> In both, gaseous monomers and either a thermal initiator or oxidant flow into a vacuum chamber and react before and while adsorbing as a growing film on the substrate. i-CVD uses heated coils above the sample to decompose a thermal initiator for the polymerization of typically vinylic monomers, while o-CVD uses heated substrates to oxidize monomers typically for conducting polymers.<sup>13,16</sup> These methods deposit conformal organic thin films on structured surfaces and shaped particles, but the high-vacuum deposition conditions limit their accessibility and, most importantly, the non-self-limiting chain reaction causes non-uniform coating thickness, especially within high aspect-ratio pores, and can lead to cauliflower-like morphology.<sup>15,17,18</sup> Prominent solution-based methods for thin polymer coatings are the layer-by-layer (LbL) deposition of charged poly-electrolytes that serves as a simple and versatile method with nanoscale control by forming self-assembled multilayers driven by electrostatic interactions, as well as surface grafting of polymers.<sup>19–23</sup> While LbL offers the highest level of topographic control, it only works with charged or highly polar polymers and, therefore, many functional hydrophobic polymers are not applicable.<sup>24</sup> Grafting is applicable to a broader variety of monomers, but similar to CVD, the chain reaction is not self-limiting and dominated by mass transport of the monomer to the growing chain, leading to faster growth at outside surfaces and slower growth deep within porous materials.

To overcome some of these challenges for porous conductive materials, we introduced the electrodeposition of polymer networks (EPoN) in prior studies as a modular approach for conformal deposition of functional polymeric ultrathin films on planar (2D) and 3D conductive substrates under mild solution conditions.<sup>12,25,26</sup> So far, EPoN has been realized by a dual-functional molecular design: non-reactive polymers with desired functionalities are modified by electrochemically active crosslinkers (eX-linkers) as chain-end groups. Importantly, the EPoN film deposition is self-limiting in its mechanism: for example, phenolate as the eX-linker end group forms radicals upon application of an oxidative potential to the substrate surface, which couple to form oligomeric crosslinks only upon continued oxidation, forming a polymer network in the immediate vicinity of the conducting surface.<sup>12,25</sup> The polymer network precipitates and adheres onto the surface as a coating. Due to its electronically insulating properties and eventual impermeability to the polymeric precursor, this results in stoppage of the charge transfer and crosslinking reaction, ceasing film growth at a condition-dependent characteristic thickness. The self-limiting deposition mechanism enables

a conformal and defect-free deposition of ultrathin polymer-network coatings on both planar and porous 3D substrates with a decoupling of the deposition chemistry from the polymer functionality.

In this work, we expand the modularity and applicability of EPoN by introducing ‘reactive’ polymers appended with eX-linker side groups. In contrast to end-group functionalized polymers, the eX-linker side groups allow for their incorporation at tunable fractions independent of polymer size. Additionally, using reactive polymers means that each monomer contains a chemical group that can be appended by a variety of functional side-groups with efficient chemical click-reactions before or after deposition. This approach reported here introduces modularity to EPoN-derived coatings since neither their function nor crosslink density is pre-determined by the original polymer, as was the case in prior EPoN studies. Thus, the reactive EPoN introduced here is beneficial for functional coatings that either cannot be synthesized as soluble polymers or are not stable under the oxidative electrodeposition conditions. Additionally, the eX-linker introduced as a randomly distributed side group endows this iteration of EPoN with broader accessibility by circumventing the synthetically challenging end-group attachment of eX-linkers demonstrated in our prior studies that is not feasible with many polymers. As a proof of this concept, we demonstrate the electrodeposition and functionalization of reactive polymer networks with poly-isoprene (PI), which contains one available alkene group (C=C double bond) in each repeating unit for various modification schemes including the thiol-ene reaction to achieve desired film properties.<sup>27</sup> We endow PI with the ability to be electrodeposited by modifying it with a small fraction of phenol side groups and demonstrate the feasibility of the post-EPoN functionalization of the resulting ultrathin PI network coatings using fluorinated alkyl thiols.

## Results and discussion

The key design principle of EPoN is a dual-functional macromolecular architecture that utilizes a small fraction of electrochemically active groups as crosslinker (eX-linker) to enable the electrodeposition of polymers as crosslinked networks. For anodic electrodeposition, phenol has proven itself an effective eX-linker for its ability to quickly couple and oligomerize upon repeated and continued oxidation to form a crosslinked polymer-network coating on the electrode surface. In our previous study, we successfully incorporated a phenolic eX-linker as the end groups of poly(ethylene oxide) and poly(*N*-isopropylacrylamide) polymers, whose properties determined the resulting coating functionality such as ionic conductivity and thermal stimuli response.<sup>12</sup> However, end-group modification of polymers exhibits various limitations: the eX-linker fraction and mesh-size are pre-determined by the polymer molecular weight and architecture, and many polymers are challenging to synthesize with desired end groups. To achieve a widely accessible and modular fabrication method for polymeric coatings, we introduce EPoN with chemically reactive polymer backbones that are modified with a small fraction of the eX-linker phenol



attached as side groups (Fig. 1a). The self-limiting film growth is mediated with an anodic potential, under which the phenolate side groups are oxidized into phenoxy radicals, the radicals couple to dimers and further continue the oxidation-coupling cycle to form oligomers. The insulating crosslinked polymer network adheres onto the electrode surface and keeps densifying, which reduces and eventually eliminates macromer permeation to the surface and stops the charge transfer reaction.<sup>25</sup> Since only a small fraction (<5 mol%) of eX-linker is required for film formation, the deposited polymer network thin film retains most of its original chemical reactivity and is amenable to modification with other functional side groups after EPoN to attain the desired film functionality (Fig. 1a).

Here, PI is selected as the reactive polymer due to its carbon–carbon double bond (C=C) in each isoprene repeating unit which supports a wide range of reaction chemistries, including thiol–ene click chemistry.<sup>28</sup> The PI used here with a molecular weight of 20 kg mol<sup>-1</sup> is 1,4-PI dominant with 7% of 3,4-isoprene units and a dispersity of 1.05 (Fig. S1a and b). The PI is modified with a small portion of 4-mercaptophenol by facile UV-

initiated thiol–ene coupling. The phenol-modified PI macroers are named PI-*x*Ph hereafter with *x* being the monomeric fraction of the phenol side group. The phenol attachment and PI-*x*Ph composition is confirmed by <sup>1</sup>H-NMR: the existence of peaks at 6.7 ppm and 7.2 ppm indicates successful incorporation of phenol, and its fraction *x* is determined by comparing the integral of phenol and backbone sp<sup>2</sup>-protons of the 1,4-PI backbone as well as the vinyl group protons of 3,4-PI (Fig. S1c). The substitution *x* is kept below 5% which is sufficient for EPoN film formation and leaves ample C=C double bonds in the polymer for post-deposition functionalization.

For its electrodeposition, ITO-coated glass is used as a planar conductive substrate and immersed in a solution of PI-*x*Ph with a stoichiometric amount of base to deprotonate the phenol groups that facilitates its oxidation. In cyclic voltammetry (CV), the phenolic side groups oxidize at a potential above -0.6 V vs. Ag/Ag<sup>+</sup>, causing polymer crosslinking and deposition on the electrode surface (Fig. 1b). The formation of the film gradually blocks the transport of the reactive PI-*x*Ph from the bulk solution to the conductive surface leading to the decrease in

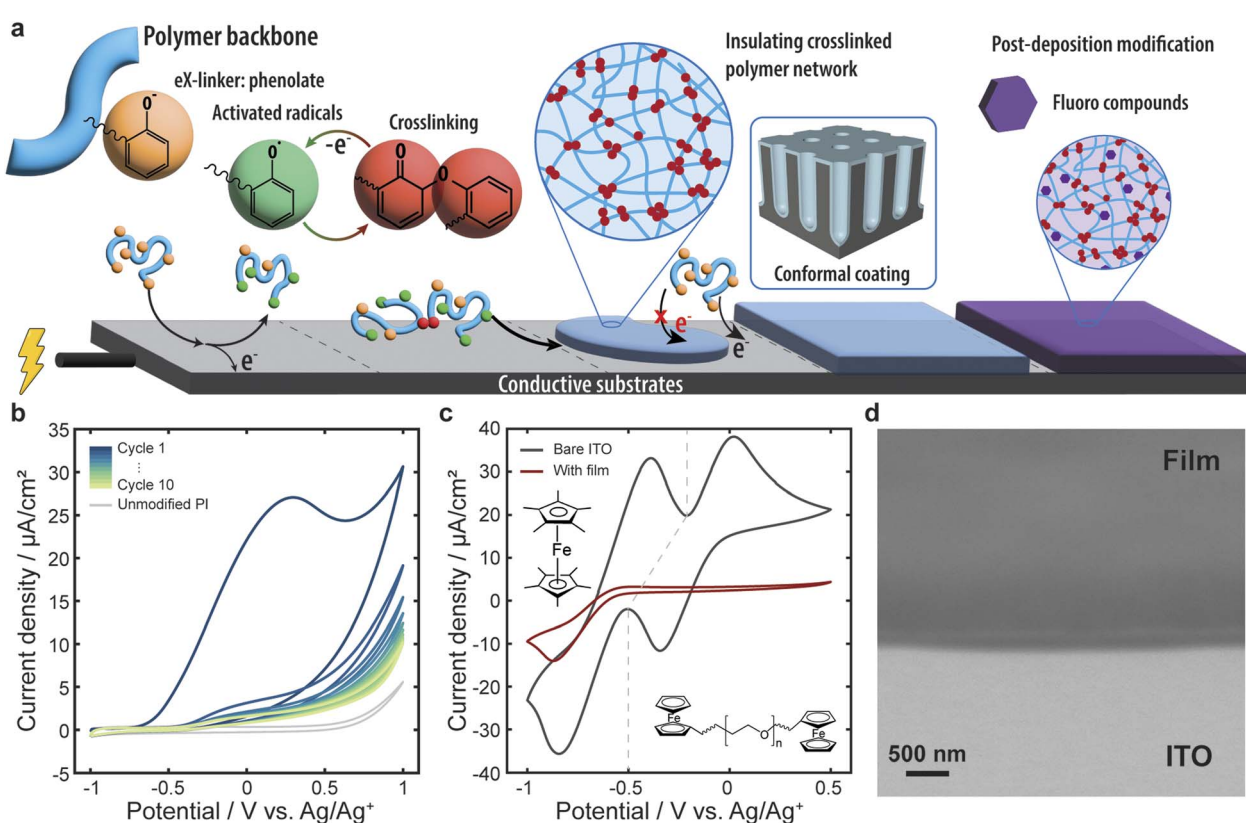


Fig. 1 (a) Scheme of the proposed self-limiting EPoN mechanism and post-deposition modification of reactive polymers appended with electrochemically activated crosslinking side groups: phenolate side groups (yellow) are oxidized at the conductive substrate to generate radicals (green) which couple into crosslinks (red), forming a polymer network on the surface. Subsequently, a functional side group is attached to the polymer network such as a fluorocarbon-thiol to the double bond of a polyisoprene coating as demonstrated here. (b) Cyclic voltammetry (CV) of a PI-2.7%Ph on an ITO-coated glass substrate, overlaid with a control CV of the same PI without phenol modification (grey), demonstrating the surface passivation caused by the irreversible phenol oxidation. (c) CVs of a solution with two distinct ferrocene-type molecules of different sizes before (black) and after (red) CV-deposition of a PI-2.7%Ph coating. The dashed line visually separates the oxidation/reduction peaks of decamethylferrocene (left) and 3.4 kDa poly(ethylene oxide)-diferrocene (right). (d) SEM image at a 45-degree angle of an EPoN-derived PI-2.7%Ph coating on ITO-coated glass.



oxidation current over successive cycles. In contrast, an unmodified PI only exhibits a small background current, indicating that the phenol side groups are the oxidizing species in the process (Fig. 1b). Due to EPoN's self-limiting mechanism, the film growth is intrinsically defect-correcting since PI-xPh will eventually diffuse to any exposed conductive area and continue oxidation and crosslinking until there is no accessible pathway to the surface left. To evaluate this lack of defects and the thin-film's molecular permeability, a CV of mixed electrochemical probe molecules with different sizes are measured before and after the CV-based EPoN of PI-2.7%Ph. The absence of oxidation current above  $-0.25$  V and reduction current above  $-0.5$  V *vs.* Ag/Ag<sup>+</sup> reveals that molecules of size similar or larger than 3.4 kg mol<sup>-1</sup> PEO are unable to reach the ITO surface, demonstrating the film is free of defects or pinholes down to the nanoscale within the electrochemical detection limit (Fig. 1c). This observation supports the mechanism that the self-limiting deposition is dominated by the hindrance of PI-xPh diffusion through the film at a critical thickness and density. The appreciable remaining redox current for decamethylferrocene (326 g mol<sup>-1</sup>) in the range of  $-1$  V and  $-0.25$  V suggests that the polymer network allows small molecules to permeate through the polymer-network thin film (Fig. 1c). This finding is important for any post-EPoN modification process to ensure penetration of functional molecules and yield functionalization throughout their thickness and not just on their surface. Lastly, the EPoN-derived PI thin films appear smooth on the ITO substrate (Fig. 1d), and the wrinkles and delamination at the film edge provide evidence that the film is not covalently bonded to the surface but adhered by Van-der-Waals forces (Fig. S1d). This distinction of EPoN to grafting of polymer brushes is beneficial for electrode coatings that require molecular permeability and access to the electrode surface, for example, which is demonstrated here with the electrochemical accessibility of decamethylferrocene even after coating of the electrode (Fig. 1c).

Since the eX-linkers are attached as side groups, the phenolic fraction may have an influence on the film properties, especially thickness, in addition to the deposition potential. To test these correlations, PI with different phenol fractions of 2.3% to 3.5% are prepared as identical solutions and deposited on ITO-coated glass at 1 V and 0.5 V *vs.* Ag/Ag<sup>+</sup>. The chronoamperometry (CA) of all PI-xPh deposited at 1 V show a rapid current decrease over the first minute and then gradually reach a steady state current over a 30 min deposition span, indicating a fast surface passivation creating a barrier to further diffusion of unreacted PI-xPh from the bulk solution (Fig. 2a). As expected from the higher concentration of electrochemically active phenol groups, both the initial and the steady-state current are higher for PI-3.5%Ph compared to PI-2.3%Ph (Fig. 2a and S2a). Similarly, the current and charge passed during EPoN at 0.5 V is lower than at 1 V *vs.* Ag/Ag<sup>+</sup> (Fig. S2b and c), even though both potentials are beyond the phenolate peak potential (Fig. 1b). This observation can be rationalized by some oxidation of PI (Fig. 1b) and the presence of water in the solution that has been shown to cause additional oxidation of the eX-linker phenol.<sup>25,29</sup>

A key metric of the composition-processing-structure-property relationships is the film thickness and uniformity. The spatially resolved film thickness is measured by interferometry and the results reveal that higher phenol fractions lead to thicker film (Fig. 2b). Interestingly, at the same phenol fraction, EPoN at 0.5 V yields significantly thicker films: a PI-2.7%Ph film from 1 V EPoN is 135 nm thick while at 0.5 V, the self-limiting film thickness is 256 nm, almost two times thicker. The same trend is observed for PI-3.5%Ph films (Fig. 2b). Interestingly, the (macro)molecular permeability test with decamethylferrocene and 3.4kDa-PEO-2Fc shows no substantial difference, indicating similar crosslink density of the final films (Fig. S2d). Thus, we hypothesize that the potential-dependent thickness is due to transient differences during film growth. Specifically, EPoN exhibits a balance between crosslinking kinetics and diffusion of both non-activated and activated (with oxidized phenolic eX-linkers) polymers to and from the surface, respectively (Fig. S3). At the lower potential of 0.5 V *vs.* Ag/Ag<sup>+</sup>, the oxidation of the phenolate groups is slower, yielding initially less activated radicals per chain. Therefore, the initial cross-linked polymer network is less dense, allowing more PI-xPh to permeate through, react at the electrode surface, and continue to grow and densify the coating until the crosslink density is reached that inhibits further polymer permeation. At 1 V *vs.* Ag/Ag<sup>+</sup>, on the other hand, the phenolate oxidation is faster and more phenolate groups are activated initially on each polymer, leading to faster crosslinking and densification of the network, resulting in a thinner film.

EPoN-derived ultrathin films are conformal and uniform on 2D substrates. On the macroscale, the average film thickness of PI-2.7%Ph is 135 nm with maximum difference of 14 nm ( $\sim 10\%$ ) across a 12 mm wide film (Fig. 2d). On the nanoscale, atomic force microscopy reveals a roughness of 3 nm over a  $10 \times 10 \mu\text{m}^2$  area with a smooth morphology (Fig. 2c). To further evaluate if the film is defect-free, electrochemical impedance spectroscopy (EIS) is carried out using a liquid metallic gallium-indium eutectic (eGaIn) soft electronic contact on top of the film. The EIS spectrum exhibits an almost vertical line in the Nyquist plot and a phase close to  $-90^\circ$  in Bode plot over all measured frequencies, the typical behavior of a plate capacitor composed of two planar conductive electrodes (ITO substrate and eGaIn contact) and a dielectric separator: the EPoN-derived ultrathin PI film (Fig. S4a and b). The measured impedance response results in a plate capacitance of 0.45 nF, which is the expected result for a plate capacitor of these dimensions. The EIS result demonstrates that the electronic resistivity of the EPoN-derived ultrathin film must be higher than  $10^{12} \Omega \text{ cm}$  and confirms that the ultrathin film is free of measurable defects and pinholes.

Since EPoN possesses a self-limiting and defect-correcting growth mechanism, ultrathin films can be conformally deposited not just on 2D but also on 3D surfaces and porous conductive substrates with EPoN. Due to the concentration dependence of the EPoN-derived coating thickness and the structural effect of 3D porous substrates on non-uniform polymer diffusion, repeating potentiostatic chronoamperometry is performed with 10 s of deposition at 1 V *vs.* Ag/Ag<sup>+</sup> followed by



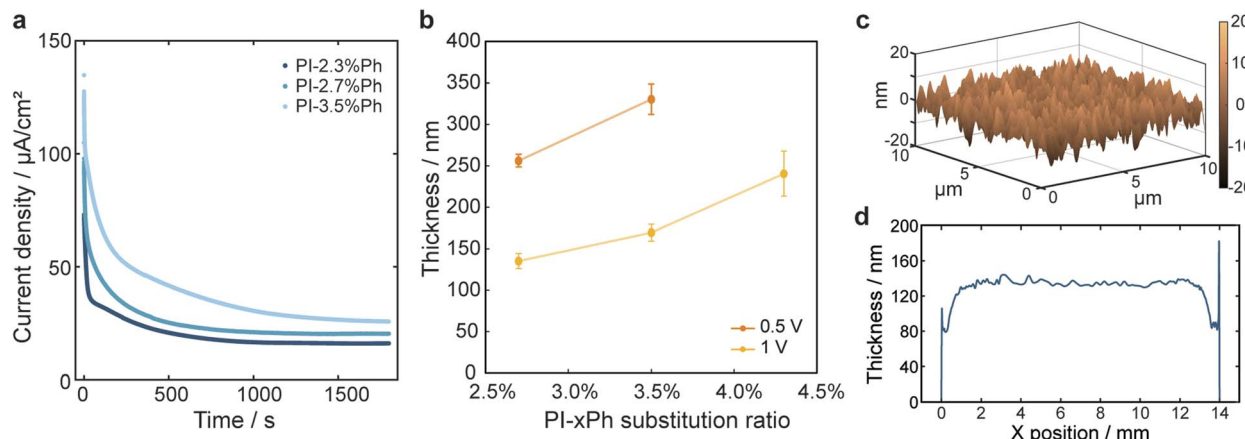


Fig. 2 (a) Chronoamperometry of the potentiostatic deposition of various PI-xPh at 1 V vs.  $\text{Ag}/\text{Ag}^+$  on ITO-coated glass. (b) Film thickness of various PI-xPh ( $x = 2.7\%$ ,  $3.5\%$ , and  $4.3\%$ ) deposited at 1 V and 0.5 V vs.  $\text{Ag}/\text{Ag}^+$ . Error bars correspond to the standard deviation of five independent thickness measurements on the same film taken at the center and in the four principal directions at a distance of 4–5 mm from the center, respectively. Lines are guide to the eye only. (c) AFM height profile of an EPoN-derived PI-2.7%Ph film at 1 V vs.  $\text{Ag}/\text{Ag}^+$  on ITO-coated glass. (d) Thickness profile across the entire film shown in (c).

50 s of rest time in between, repeated 360 times. The interval time is set to give the active polymeric species adequate time to diffuse into the pores and compensate for the concentration gradient due to the PI consumption in the previous cycle. To this end, PI-2.7%Ph is coated on a 3D-structured carbon with low-tortuosity channel-like pores that exhibit an average pore diameter of 5–9  $\mu\text{m}$  and dense carbon walls between the pores. The deposition current decreases with proceeding cycles and after 240 cycles, the current and passed charge show negligible cycle-to-cycle difference, indicating the surface is fully passivated and deposition has concluded (Fig. 3a and S5a). The coating on the porous 3D carbon also shows blockage of the macromolecular redox probe, confirming the complete passivation of the carbon surface area (Fig. 3b).

Cross-sectional SEM images show that the EPoN-derived PI-2.7%Ph ultrathin film conformally coats the high aspect-ratio micron-sized pores with a decreasing thickness from the pore end at 258 nm ( $N = 5$  for all thickness measurements on 3D carbon electrodes) to 138 nm at the pore entrance (Fig. 3c and Table S1). Unexpectedly, the PI-2.7%Ph film deposited onto a hierarchically porous carbon with both micron-scale channel-like pores and nanoscale pores in the walls manifest an opposite trend with a thicker coating at the entrance (630 nm) and thinner at the pore end (260 nm) (Fig. S5b and Table S1). We hypothesize that for 3D carbon electrodes, both the diffusion of unreacted PI-xPh into the pores and the coupled oligomers away from the electrode vicinity is affected by the pore structure. Diffusion of coupled but soluble polymer clusters as well as

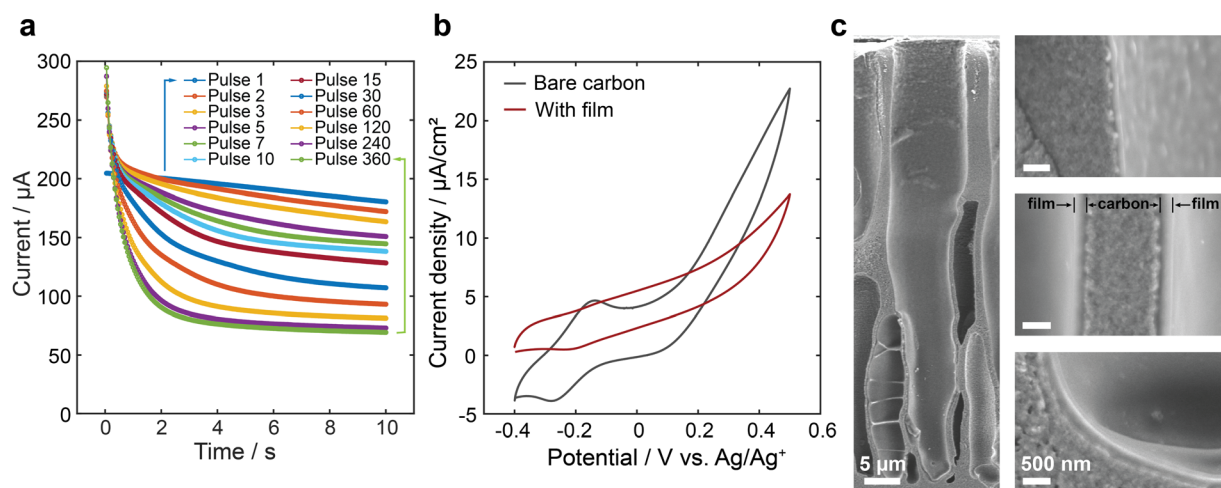


Fig. 3 (a) Current of sorted 10 s pulses from the EPoN of PI-2.7%Ph. (b) CVs before and after the deposition shown in (a) on a solution containing DMFc and 3.4 kDa-PEO-2Fc. (c) SEM cross-sectional images of PI-2.7%Ph coated on a dense-wall 3D carbon substrate. Left image shows the cross-sectional image over the full pore length (scale bar: 5  $\mu\text{m}$ ) and right images are higher magnification images (scale bar: 500 nm) at the pore entrance (top), middle (middle), and end (bottom). The grainy darker parts are the 3D carbon substrate, and the smooth lighter areas correspond to the EPoN-derived PI coating.



activated oxidized polymers are confined within the pore, potentially leading to enhanced contribution to the film mass inside the pore than at its entrance, where diffusion into the bulk solution leads to a loss of activated and small crosslinked polymer network fragments.<sup>26</sup> This hypothesis explains thicker films at the pore end than entrance for EPoN, as observed here for the dense carbon. However, the case for the hierarchical 3D carbon with nanopores in the wall shows the opposite result. This electrode is 200  $\mu\text{m}$ , more than 3 times thicker than the dense 3D carbon, and nanoporosity further leads to higher electronic resistance across the carbon electrode. Thus, it is possible that the PI-xPh in solution experiences a potential gradient from pore end to the pore entrance due to ohmic resistance of the electrode, and our observation on planar electrodes that lower potential yields thicker films could explain this phenomenon, though this is purely speculative at this point. Importantly, no distinguishable film growth is observed in the nanopores of the walls that are open to the channel surfaces, which implies that the fast film growth quickly blocks the nanopore entrance to the PI-xPh and hinders film deposition inside the nanoporous walls (Fig. S5c). Some wrinkling of the coating and film delamination from the pore walls after fracturing of the hierarchically porous 3D carbon electrode further suggests that the adhesion between the substrate and the film is based on non-covalent Van-der-Waals forces, which might allow for a broader choice of substrate materials for EPoN over sensitive electrografting procedures (Fig. S5d).

To validate the capability of post-EPoN functionalization of the PI-xPh coatings, a fluorine-rich molecule with a thiol group is utilized since C-F bonds can be quantitatively detected by X-ray photoelectron spectroscopy (XPS). The chemical modification of the coating is realized by UV-initiated thiol–ene coupling between 1H,1H,2H,2H-perfluorodecanethiol (PFDT) and an EPoN-derived PI-3.5%Ph ultrathin film on ITO-coated glass (Fig. 4a). The modified film is thoroughly cleaned with dimethyl formamide and chloroform, both good solvents for PFDT. The emergence of C-F3 and C-F2 peaks at 291.5 and 294 eV in the

high-resolution C1s spectrum suggests the successful incorporation of the fluorinated side group after only a short 90 s UV exposure (Fig. 4b). The integral of fitted peaks occupies 16 atomic percentage (atom%) which corresponds to a conversion of 12.5% of the crosslinked PI network's double bonds. To evaluate the uniformity of the modification through the thickness of the EPoN-derived ultrathin film, depth profiling using ion-cluster etching is employed that shows a slight decrease in the atomic percentage of C-F with depth reaching a constant value deeper into the film (Fig. S6a–c). The results demonstrate that the efficiency of the post-deposition modification reduces somewhat with depth, which may be caused by limited penetration of PFDT molecules into the film. We also note that the polyisoprene used here obtained from anionic polymerization is composed of 93% of 1,4-PI and 7% of 3,4-PI, which contributes to the low conversion efficiency. The thiol–ene reactivity of in-chain 1,4-units is up to ten times lower than pendant terminal double bonds, while in-chain double bonds also have increased propensity to inter-chain crosslinking under thiol–ene conditions even in solution, an effect that is likely amplified in already crosslinked EPoN-derived films.<sup>30,31</sup>

Further, the thickness of the modified film area decreases from 206 nm to 99 nm while the thickness of the same film outside the modification area only decreases by 13 nm. We postulate that UV irradiation-induced double-bond cleavage, a process that is promoted by thiyl radicals, is the reason for the loss in film thickness.<sup>32</sup> This hypothesis is further supported by the complete film removal observed after pro-longed UV exposure of 10 minutes, while a slower decrease in film thickness accompanied by increased propensity to swelling is observed upon UV exposure of an EPoN-derived PI-3.5%Ph film soaked in pure DMF and exposed to UV. Thus, under the modification conditions employed here, 12.5% of double bond conversion may be the limit, but future application of PI-based post-EPoN functionalization can be improved by increasing the fraction of 3,4-PI to yield higher conversion, combined with milder

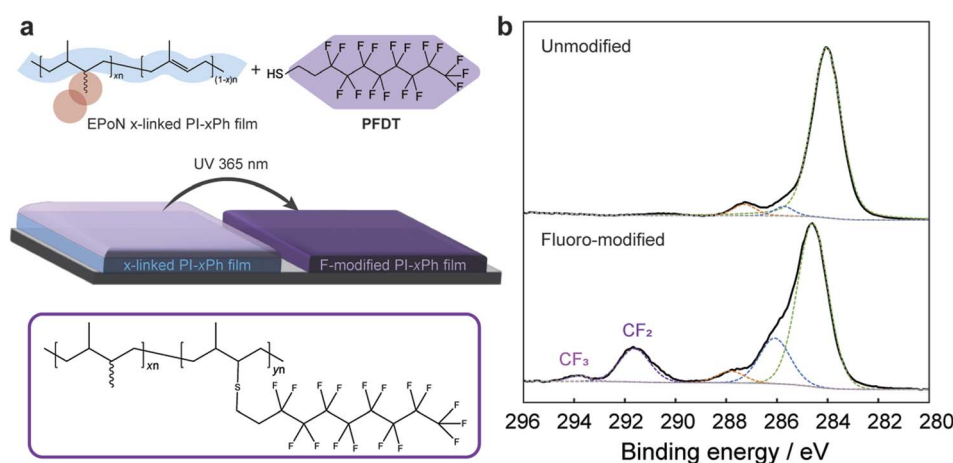


Fig. 4 (a) Scheme of the post-EPoN functionalization process using the thiol–ene reaction between the PI coating and a fluorocarbon thiol. (b) High resolution C1s X-ray photoelectron spectroscopy (XPS) scans of an EPoN-derived PI-3.5%Ph ultrathin film before (top) and after (bottom) fluorocarbon functionalization (y-axis: electron count).



protocols that avoid UV-induced chain scission, such as thermally induced thiol–ene reactions.<sup>30</sup>

To test the stability of the reactive EPoN-derived PI- $x\%$ Ph thin films and fluoro-modified coatings, thickness and XPS of the samples in Fig. 2b and 4b are measured after storage in ambient conditions for 120 days. The thickness results show negligible difference over the 120-day period (Fig. S7a and Table S2), while the XPS data reveals a shift to and increase in intensity at higher binding energies, suggesting the presence of more oxidized carbon–carbon and carbon–oxygen bonds. This indicates that the films undergo slow oxidation in ambient air over a 120-day period (Fig. S7b), as expected for unsaturated organic thin films without stabilizers such as radical or oxygen scavengers.

We further set out to expand the substrate choices for our EPoN method to oxidatively unstable metals, for example, by introducing a reductive eX-linker: arylbromide (ArBr) in the form of bromothiophenol. The proposed cathodically mediated crosslinking mechanism of bromobenzene eX-linker at reductive potentials involves the dehalogenation of the aromatic system and generation of a benzyl radical, which can couple to another activated benzyl radical to form a dimeric crosslink<sup>33</sup> (Fig. S8a). The cyclic voltammetry of a 100 mg mL<sup>-1</sup> bromobenzene modified PI (PI-9%ArBr) shows lower reductive currents than the oxidative current observed for phenol. Additionally, the decrease in current is small over repeated cycles (Fig. S8b). Although the XPS C1s spectrum shows a signal, the thickness measured by ellipsometry suggests a 3 nm thin layer which cannot be distinguished from electrografting or organic residue after cleaning of the EPoN-coated substrate (Fig. S8c). In another attempt, EPoN is carried out in concentrated PI-6%ArBr solution (300 mg mL<sup>-1</sup>) at  $-3$  V vs. Ag/Ag<sup>+</sup> on a gold substrate for 8 h. The obtained film is substantially thicker but not uniform, with film thickness ranging from 8 nm at the edge to 200 nm in the center (Fig. S8d and Table S3). These results suggest that the slow coupling kinetics of this system, potentially stemming from side-reactions of the cathodically formed benzyl radical, renders benzyl bromide not as a suitable eX-linker for EPoN.

## Conclusion

In this manuscript, we report the next generation of EPoN as a general fabrication method to coat conductive materials of arbitrary shape with ultrathin polymer films. Specifically, we introduce EPoN of reactive polymers appended with electrochemical crosslinkers as side groups that enables size-independent tuning of crosslink density and deposition-independent functionalization of the resulting coatings after their deposition. This concept is exemplified with polyisoprene containing less than 5% phenolic side groups that exhibits the EPoN-defining surface passivation and self-limiting growth behavior resulting in conformal coatings on both planar and 3D conductive substrates. The coating thickness is tunable on the sub-micron length scale through deposition potential and phenol fraction. Importantly, the preservation of the alkene group of the PI during EPoN enables its facile post-deposition

functionalization demonstrated by the emergence of the prominent C–F bond after 90 s of UV-induced thiol–ene modification with a fluorinated mercaptan. This reactive EPoN method substantially expands the applicability of this method by increasing accessible functionalities for conformal ultrathin polymeric coatings through facile small-molecule modification after film deposition. Importantly, the attachment of the electrochemically activated crosslinker unit as a side group follows the same facile reaction type, rendering the full process accessible to a wide range of scenarios. We envision that the general concept of EPoN with reactive polymers will expand to other reactive polymer choices and copolymer architectures. The versatility of this reactive EPoN has great potential in numerous applications fields including protective surface coatings, sensors, or energy storage, but also for accelerated polymer material discovery.<sup>34</sup>

## Experimental section

### Materials

Isoprene (>99%), *n*-butyllithium (2.5 M in hexanes), sec-butyllithium solution (1.4 M in cyclohexane), 1,1-diphenyl ethylene (97%), tetrahydrofuran (>99.9% anhydrous, contains 250 ppm BHT as inhibitor), benzene (anhydrous, 99.8%), 2-hydroxy-2-methylpropiophenone (Darocur 1173, 97%), 2,2'-(ethylenedioxy)diethanethiol (95%), pentaerythritol tetrakis(3-mercaptopropionate) (>95%), tri(ethylene glycol) divinyl ether (98%), bis(pentamethylcyclopentadienyl)iron(II) (97%), vinyl-ferrocene (97%), poly(acrylonitrile) (PAN,  $M_w$  = 150 kg mol<sup>-1</sup>), polyvinyl pyrrolidone (PVP,  $M_w$  = 40 kg mol<sup>-1</sup>), 1,1,2,2,2H-perfluorodecanethiol (97%), deuterated chloroform (CDCl<sub>3</sub>), indium–gallium eutectic (eGaIn, gallium 75.5%, indium 24.5%,  $\geq$ 99% trace metal basis), silver wire (diam. 0.5 mm, 99.9% metal basis), *N*-methyl-2-pyrrolidone (NMP) and poly(vinyl alcohol) (31–50 kg mol<sup>-1</sup>, 81–89% hydrolyzed) were purchased from Sigma-Aldrich. Poly(ethylene glycol) dithiol ( $M_w$  = 3.4 kg mol<sup>-1</sup>) was purchased from Biopharma. Dimethylformamide (DMF, anhydrous), dimethyl sulfoxide (DMSO, certified ACS), chloroform (anhydrous), methanol ( $\geq$ 99.9%, HPLC), lithium hydroxide (98%, anhydrous), tetrabutylammonium perchlorate (TBAP, 98%), silver perchlorate (anhydrous), indium-tin-oxide (ITO) coated glass ( $R_s$  = 70–100 Ohm/□, roughness: Ra = 0.8 nm), platinum wire (diam. 0.25 mm, 99.9% trace metal basis) and silicon wafers were purchased from Fisher Scientific. Carbon black and stainless steel were supplied by Fuel Cell Earth and MTI Corporation, respectively.

### Preparation of eX-linker modified polyisoprene (PI- $x$ Ph & PI- $x$ ArBr)

Polyisoprene homopolymer (PI), was synthesized *via* living anionic polymerization.<sup>35</sup> Briefly, the monomer isoprene was purified with *n*-butyllithium after removal of its cyclohexane solvent, freeze-pump-thawed three times, and distilled using a high-vacuum Schlenk line prior to use. Polymerization of PI was performed in benzene (purified with *n*-butyllithium/1,1-diphenyl ethylene and distilled) in a Schlenk flask under



nitrogen atmosphere, initiated by sec-butyllithium at pre-determined molar ratios to the isoprene monomer. The benzene/sec-butyllithium mixture was stirred for several hours before the isoprene was added and then continuously stirred overnight at room temperature. Freeze-pump-thawed methanol was added to terminate the polymerization. Subsequently, the solvents were removed from the mixture *via* rotary evaporator and the resulting colorless solid was redissolved in chloroform at approximately 20 wt% followed by two cycles of precipitation into cold methanol, filtration, and redissolving. The purified products were dried in a vacuum oven at 50 °C for 3 days to yield PI as colorless and rubbery solid.

For its modification with eX-linkers, PI was dissolved in chloroform at a concentration of 50 mg mL<sup>-1</sup> followed by the addition of 4-mercaptophenol (for phenol-modified PI) or 4-bromothiophenol (for bromobenzene-modified PI) and radical photo-initiator Darocur 1173 with a molar ratio to isoprene unit of 20%. The solution was saturated with nitrogen by bubbling for 15 min then transferred to a septum-capped UV-transparent cuvette and exposed to 302 nm UV for 72 h. The resulting solution was concentrated by rotary evaporator to a concentration of approximately 150–200 mg mL<sup>-1</sup> and precipitated in 0 °C methanol, centrifuged at 4000 rpm for 10 min to separate the viscous polymer phase at the bottom and reconstituted to 150 mg mL<sup>-1</sup>. The purification process was repeated twice. The purified product was dried in a desiccator for 24 hours and the eX-linker fraction was quantified by proton-nuclear magnetic resonance (<sup>1</sup>H-NMR) spectroscopy using an Agilent 400 MHz VNMRS spectrometer. The resulting copolymers with eX-linkers are termed PI-xPh and PI-xArBr for phenol- and bromobenzene-modified PI, respectively, where *x* represents the monomer fraction of eX-linker in percent.

### Porous 3D carbon fabrication

Free-standing porous 3D carbon electrodes were prepared by non-solvent induced phase separation (phase inversion) of PAN followed by carbonization similar to previous reports.<sup>36</sup> Briefly, polymer dope solutions of PAN, DMSO, and water at a mass ratio of 1.4:10.3:1 for dense low-tortuosity 3D carbon electrodes and of PAN, PVP, DMSO, and DMF at a mass ratio of 1:1:4:4 for hierarchically porous 3D carbon were prepared and thoroughly stirred at 70 °C until fully dissolved and homogeneous. The polymer dope solutions were cast on an organogel substrate to ensure open and accessible low-tortuosity pores. The organogel was prepared by mixing 2,2'-(ethylenedioxy)diethanethiol, pentaerythritol tetrakis(3-mercaptopropionate), tri(ethylene glycol) divinyl ether at a mass ratio of 13.78:1:16.12, respectively, resulting in a 1:1 stoichiometric ratio of thiol to vinyl end groups. Darocur 1173 was added at 1.4 wt% as a photoinitiator. 0.8 mL of the solution was then pipetted on a glass microscope slide to coat it. Then the solution was exposed to 365 nm UV for 3 min to form the organogel. The polymer dope solutions were spread with a doctor blade (BYK-Gardener) onto a glass slide coated with the cross-linked organogel and subsequently submerged in a nonsolvent bath of either deionized water (hierarchically porous carbon) or 1:1

water:isopropanol mixture (dense low-tortuosity 3D carbon) at 21 °C for 10 minutes to induce phase inversion by non-solvent/solvent exchange. The resulting porous polymer films were transferred to room-temperature deionized water overnight to ensure completion of the solvent extraction. Afterwards, the films were placed between two sheets of paper towel and dried in a vacuum oven at 70 °C for 12 hours. For carbonization, the polymer films were sandwiched between graphite plates and placed in a tubular furnace first held between 250–280 °C under air for cyclization of the PAN backbone and then heated to 1100 °C under Argon flow to carbonize.

### Electrodeposition of reactive polymer networks (EPoN)

The PI-xPh was dissolved at 100 mg mL<sup>-1</sup> in THF with TMAH x5H<sub>2</sub>O at a 1:1 molar ratio to phenol groups and 0.1 M of supporting electrolyte TBAP. Platinum wire was used as the counter electrode, and silver wire as the frit-separated reference electrode immersed in a silver reference solution composed of 0.05 M of AgClO<sub>4</sub> and 0.1 M of TBAP in THF. All electrochemical experiments were carried out on a Gamry Reference 600+ potentiostat. Cyclic voltammetry (CV) of PI-xPh on planar ITO substrates was performed between -1 V and +1 V vs. Ag/Ag<sup>+</sup> at 50 mV s<sup>-1</sup> for 10 cycles while only 3 cycles were applied for unmodified PI as a control. Potentiostatic electrodeposition with chronoamperometry (CA) was conducted at +1 V vs. Ag/Ag<sup>+</sup> for all PI-xPh on ITO substrates. All electrodeposited films were rinsed with THF three times and blow-dried with air.

Reductive EPoN was performed with PI-xArBr in 0.1 M TBAP in THF. CV deposition was performed at 100 mg mL<sup>-1</sup> polymer in a range between -2.5 V and -0.5 V vs. Ag/Ag<sup>+</sup>. For potentiostatic deposition, PI-xArBr concentration was elevated to 300 mg mL<sup>-1</sup> and -3 V was used in chronoamperometry for 8 hours duration.

For the electrodeposition on 3D porous carbon electrodes, repeating potentiostatic chronoamperometry was performed with 10 s deposition at +1 V vs. Ag/Ag<sup>+</sup> followed by a 50 s rest at open circuit voltage to allow for polymer to diffuse from the bulk solution into the pores. The process was repeated for 360 cycles to achieve a total deposition time of 1 h. After deposition, the films are soaked in THF for 2 hours and washed thoroughly 5 times and dried in a desiccator for 16 h.

### Post-functionalization of EPoN-derived PI-xPh ultrathin films

One drop (20 μL) of pure 1H,1H,2H,2H-perfluorodecanethiol (PFDT) was applied on top of EPoN-derived PI-xPh films. The film with PFDT was exposed to 365 nm UV with an intensity of 27 W cm<sup>-2</sup> from the top for 90 s using an OmniCure LX500 spot UV lamp. The functionalized film was washed with DMF and rinsed with chloroform 3 times each and blow-dried with air.

### Characterization

To test the surface passivation and molecular permeability, CVs were performed between -1 V and +0.5 V vs. Ag/Ag<sup>+</sup> at a scan rate of 25 mV s<sup>-1</sup> before and after EPoN with a mixed probe solution containing with 0.001 M decamethylferrocene (DMFc) and 0.001 M of 3.4k-PEO-2Fc in THF with 0.1 M TBAP as



supporting electrolyte. The preparation of the macromolecular probe ferrocene 3.4k-PEO-2Fc was introduced in our previous study.<sup>12</sup>

Electrochemical impedance spectroscopy (EIS) measurements were performed on a Gamry Reference 600+ potentiostat using an eGaIn drop as a soft contact with a contact area of 3.14 mm<sup>2</sup>. A signal amplitude of 10 mV around the open circuit potential over the frequency range of 0.1 Hz to 2 MHz was employed.

The line profile and film thickness were measured with a Filmetrics F40-UVX 6 interferometer, thickness values were extracted from fitting the results to a polymer model with initial refractive index guess of 1.5.

Film roughness measurements were carried out on an Asylum Research MFP-3D Infinity Atomic Force Microscope (AFM) using alternating contact mode and with a scanning area of 10 × 10 μm<sup>2</sup>. The scan used an aluminum cantilever at 0.3 Hz scan speed and 256 lines/points. The roughness was directly obtained from the software which calculates the average roughness (Ra) across the whole area.

Scanning electron microscopy (SEM) on the films was conducted on a Zeiss Supra 55 FE SEM and a Zeiss Gemini 360 FE SEM with an electron beam accelerating voltage of 3 kV using a secondary electron detector.

X-Ray photoelectron spectroscopy (XPS) was performed on a Thermo Scientific K-Alpha + XPS system. The carbon binding energy measurement was taken using a 400 μm spot size X-ray gun and 50 eV pass energy for high resolution scans with five scans and 25 s dwell time per spectrum. The depth profile was acquired by argon ion cluster etching for 20 cycles where the Ar1000+ with 8000 eV and etching time of 30 s was used to etch 27 nm through the film.

## Author contributions

WW and JGW conceptualized and designed the research plan. YL synthesized the polymer. WW and ZZ performed the polymer modification. WW performed the electrodeposition, functionalization, characterization of the thin films, and all data analysis. AR and JY fabricated the porous carbon electrodes. WW wrote the first draft of the manuscript. WW and JGW revised the manuscript for publication. JGW supervised the research project.

## Conflicts of interest

The authors declare no conflict of interest. JGW, WW, and ZZ are inventors of a provisional patent application related to this research that has been filed by Boston University.

## Data availability

The data supporting this article have been included as part of the SI.

Supplementary information is available with H-NMR spectra and GPC of the polymers, additional SEM on planar ITO and 3D carbon electrodes, additional electrochemical deposition and

permeability data, EIS spectra, tables with film thickness, additional XPS data depth- and time-resolved, as well as data on cathodic EPoN with bromobenzene (ArBr) side groups. See DOI: <https://doi.org/10.1039/d5ta03811a>.

## Acknowledgements

This material is based upon work supported by the National Science Foundation under Grant No. CBET-2146597. The research was in part sponsored by the Army Research Office and was accomplished under Cooperative Agreement Number W911NF-25-2-0074. The views and conclusions contained in this document are those of the authors and should not be interpreted as representing the official policies, either expressed or implied, of the Army Research Office or the U.S. Government. This work was performed in part at the Harvard University Center for Nanoscale Systems (CNS); a member of the National Nanotechnology Coordinated Infrastructure Network (NNCI), which is supported by the National Science Foundation under NSF award no. ECCS-2025158.

## References

- 1 K. Zhao, M. Li, H. Geng, Z. Gao, X. Zhang, K. P. C. Sekhar, P. Zhang and J. Cui, *Biomacromolecules*, 2024, **25**, 6727–6736.
- 2 A. Hozumi, K. Ushiyama, H. Sugimura and O. Takai, *Langmuir*, 1999, **15**, 7600–7604.
- 3 M. Xia, T. Yang, S. Chen and G. Yuan, *Colloid Interface Sci. Commun.*, 2020, **36**, 100264.
- 4 Y. Tian, H. Li, M. Wang, C. Yang, Z. Yang and X. Liu, *Prog. Org. Coat.*, 2021, **151**, 106043.
- 5 S. S. Hoseini, A. Seyedkanani, G. Najafi, A. P. Sasmito and A. Akbarzadeh, *Energy Storage Mater.*, 2023, **59**, 102768.
- 6 S. Kausar, M. Yousaf, S. Mir, N. S. Awwad, H. A. Alturaifi and F. Riaz, *Electrochem. Commun.*, 2024, **169**, 107836.
- 7 Y. Li, Z.-Y. Fu and B.-L. Su, *Adv. Funct. Mater.*, 2012, **22**, 4634–4667.
- 8 N. Linares, A. M. Silvestre-Albero, E. Serrano, J. Silvestre-Albero and J. García-Martínez, *Chem. Soc. Rev.*, 2014, **43**, 7681–7717.
- 9 C. M. A. Parlett, K. Wilson and A. F. Lee, *Chem. Soc. Rev.*, 2013, **42**, 3876–3893.
- 10 A. Sharma, S. B. Eadi, H. Noothalapati, M. Otyepka, H.-D. Lee and K. Jayaramulu, *Chem. Soc. Rev.*, 2024, **53**, 2530–2577.
- 11 A. R. Nabais, S. Ahmed, M. Younis, J.-X. Zhou, J. R. Pereira, F. Freitas, D. Mecerreyres, J. G. Crespo, M.-H. Huang, L. A. Neves and L. C. Tomé, *J. Membr. Sci.*, 2022, **660**, 120841.
- 12 W. Wang, A. B. Resing, K. A. Brown and J. G. Werner, *Adv. Mater.*, 2024, **36**, 2409826.
- 13 M. Heydari Gharahcheshmeh and K. K. Gleason, *Adv. Mater. Interfaces*, 2019, **6**, 1801564.
- 14 P. Kovacik, G. del Hierro, W. Livernois and K. K. Gleason, *Mater. Horiz.*, 2015, **2**, 221–227.
- 15 K. K. Gleason, *Adv. Mater.*, 2024, **36**, 2306665.
- 16 S. J. Yu, K. Pak, M. J. Kwak, M. Joo, B. J. Kim, M. S. Oh, J. Baek, H. Park, G. Choi and D. H. Kim, *Adv. Eng. Mater.*, 2018, **20**, 1700622.



17 K. K. Lau and K. K. Gleason, *Macromolecules*, 2006, **39**, 3688–3694.

18 K. W. Park, K. K. Gleason and R. Yang, *Adv. Funct. Mater.*, 2024, 2417620.

19 E. Pinto, M. Barsan and C. Brett, *J. Phys. Chem. B*, 2010, **114**, 15354–15361.

20 D. Rawtani and Y. K. Agrawal, *Nanobiomedicine*, 2014, **1**, 8.

21 D. Belanger and J. Pinson, *Chem. Soc. Rev.*, 2011, **40**, 3995–4048.

22 A. J. Magenau, N. C. Strandwitz, A. Gennaro and K. Matyjaszewski, *Science*, 2011, **332**, 81–84.

23 J. O. Zoppe, N. C. Ataman, P. Mocny, J. Wang, J. Moraes and H. A. Klok, *Chem. Rev.*, 2017, **117**, 1105–1318.

24 J. J. Richardson, M. Björnalm and F. Caruso, *Science*, 2015, **348**, aaa2491.

25 W. Wang, Z. Zheng, A. B. Resing, K. A. Brown and J. G. Werner, *Mol. Syst. Des. Eng.*, 2023, **8**, 624–631.

26 Z. Zheng, A. B. Resing, W. Wang and J. G. Werner, *RSC Appl. Polym.*, 2024, **2**, 1139–1146.

27 F. A. Soares and A. Steinbüchel, *Macromol. Biosci.*, 2021, **21**, 2100261.

28 L. Laysandra, D. Bazliah, A. Njotoprajitno, K.-L. Chen and Y.-C. Chiu, *ACS Appl. Polym. Mater.*, 2025, **7**, 1921–1933.

29 M. Gattrell and D. W. Kirk, *J. Electrochem. Soc.*, 1992, **139**, 2736.

30 J. Justynska, Z. Hordyjewicz and H. Schlaad, *Polymer*, 2005, **46**, 12057–12064.

31 N. Ten Brummelhuis, C. Diehl and H. Schlaad, *Macromolecules*, 2008, **41**, 9946–9947.

32 F. A. Soares and A. Steinbüchel, *Eur. Polym. J.*, 2022, **165**, 111001.

33 X. Wang, J. Wu, H. Liu, F. Kang, F. Yan and Q. Zhang, *Macromolecules*, 2023, **56**, 10198–10205.

34 H. Quinn, W. Wang, J. G. Werner and K. A. Brown, *Anal. Methods*, 2023, **15**, 3592–3600.

35 Y. Li, A. Plummer and J. G. Werner, *ACS Nano*, 2024, **18**, 19150–19160.

36 A. B. Resing, C. Fukuda and J. G. Werner, *Adv. Mater.*, 2023, **35**, 2209694.

